



1 **Diel and seasonal methane dynamics in the shallow and** 2 **turbulent Wadden Sea**

3

4 Tim R. de Groot ¹, Anne M. Mol ¹, Katherine Mesdag ², Pierre Ramond ^{1,3}, Rachel Ndhlovu ¹,
5 Julia C. Engelmann ¹, Thomas Röckmann ² and Helge Niemann ^{1,4,5}

6 1. Royal Netherlands Institute for Sea Research (NIOZ), Texel, the Netherlands

7 2. Institute for Marine and Atmospheric Research Utrecht (IMAU), Utrecht University, Utrecht, The Netherlands

8 3. Instituto de Ciencias del Mar (ICM), Barcelona, Spain

9 4. Department of Earth Sciences, Utrecht University, Utrecht, The Netherlands

10 5. Centre of Arctic Gas Hydrate, Environment and Climate (CAGE), UiT the Arctic University of Norway,
11 Tromsø, Norway

12

13 Correspondence to: Tim de Groot (tim.de.groot@nioz.nl)

14

15 **Abstract.** The Wadden Sea is a coastal system fringing the land-sea borders of Denmark, Germany, and the
16 Netherlands. The Wadden Sea is extremely productive and influenced by strong variations in physical and
17 biological forcing factors that act on time scales of hours to seasons. Productive coastal seas are known to dominate
18 the ocean's methane emission to the atmosphere, but knowledge on controls and temporal variations of methane
19 dynamics in these vastly dynamic systems are scarce. Here we address this knowledge gap by measuring methane
20 inventories and methanotrophic activity at a temporal resolution of two hours over a time period of two days,
21 repeatedly during four successive seasons in the central Dutch Wadden Sea. We found that methane dynamics
22 varied between colder and warmer seasons, with generally higher water column methane concentrations and
23 methanotrophic activity in the warmer seasons. Efflux of methane to the atmosphere was, on the other hand, lower
24 in the warmer seasons because of lower wind speeds. On a diel scale, tides controlled methanotrophic activity,
25 which increased ~ 40 % at low tide compared to high tide. We estimate that methane oxidizing bacteria reduce the
26 methane budget of the Dutch Wadden Sea by only 2 %, while ~ 1/3 escapes to the atmosphere and ~ 2/3 are flushed
27 out into the open North Sea at ebb tide. Our findings indicate that tides play a key role in controlling methane
28 dynamics and methanotrophic activity and highlight the importance of high resolution and repeated sampling
29 strategies to resolve methane dynamics in fast-changing coastal systems.



30 **1 Introduction**

31

32 **1.1 Methane and methane oxidation**

33 Atmospheric methane (CH₄) concentrations have been increasing since industrial times, surpassing 1900 ppb in
34 2021 (Lan et al., 2022) and contributing more than 20 % of total radiative forcing in the atmosphere (Etminan et
35 al., 2016). Due to its relative short atmospheric lifetime of ~10 years (Canadell et al., 2021), reducing methane
36 emissions to the atmosphere could play a key role in global warming mitigation strategies. However,
37 implementation of such strategies requires a thorough understanding of methane sources and sinks. Anthropogenic
38 methane emissions (336 – 376 Tg y⁻¹) are rather well constrained and constitute ~60 % of the total atmospheric
39 budget, but large uncertainties exist around the strength of individual natural sources (Saunio et al., 2020).
40 Especially, methane emissions from marine environments (5 -28 Tg CH₄ y⁻¹) are not well constrained (Weber et
41 al., 2019; Rosentreter et al., 2021).

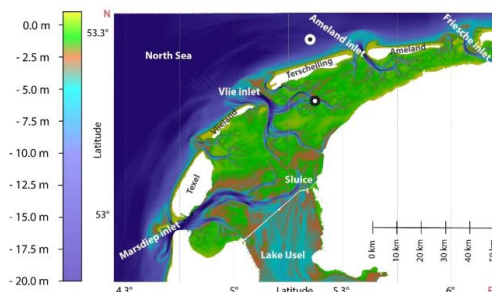
42 The inner shelf (0 – 50 m water depth) only account for ~ 3 % of the global ocean surface but are a main source
43 of marine methane emissions to the atmosphere (Weber et al., 2019). In these shallow ecosystems, light availability
44 as well as terrestrial inputs of nutrients support a high diversity of producers and consumers that generate huge
45 quantities of organic matter (Philippart et al., 2009; Beck and Brumsack, 2012). Consequently, rates of organic
46 matter degradation, including methanogenesis in anoxic sediments are high, often leading to elevated levels of free
47 and dissolved methane in sediments and pore waters (Bange et al., 1994; Røy et al., 2008; Wu et al., 2015).
48 Transport of methane-rich porewaters and ebullition of methane bubbles, in return, lead to elevated methane
49 concentrations in the water column (Reeburgh, 2007; Grunwald et al., 2009; James et al., 2016). It is estimated
50 that ~ 5 % of shelf seas surface waters have methane concentrations above 100 nM (Weber et al., 2019).
51 Nevertheless, a substantial amount of dissolved methane is oxidized by aerobic methanotrophic bacteria (MOB),
52 which mediate the aerobic oxidation of methane (MOx) (Reeburgh, 2007):



54 Similar to other metabolic processes involving small molecules, MOx discriminates against isotopically heavy
55 methane (i.e. containing ¹³C and ²H (D) instead of ¹²C and ¹H) so that the residual methane pool successively
56 becomes ¹³C and D enriched as a result of ongoing MOx (Barker and Fritz, 1981; Whiticar, 1999).

57 MOB typically belong to the Gamma- (type I and type X), Alphaproteobacteria (type II), Verrucomicrobia and
58 members of candidate division NC10 (Hanson and Hanson, 1996; Knief, 2015). MOBs build a microbial methane
59 filter in the water column that functions as the ultimate sink for oceanic methane before reaching the atmosphere.
60 Yet, little is known about the controls and capacity of this microbial filter in the inner shelf ecosystems where the
61 vertical distance between the sedimentary source and the atmosphere is short. Factors such as oxygen (Boetius and
62 Wenzhöfer, 2013; Steinle et al., 2017) and methane availability (Mau et al., 2013; James et al., 2016) affect MOx,
63 but also increasing water temperatures play a role by impacting metabolic rates of MOB (He et al., 2012). The
64 capacity of the microbial MOB filter increases with continuity in the water column (Steinle et al., 2015; James et
65 al., 2016). However, water mass movement induced by temperature changes and wind leads to shifting mixing
66 regimes that disrupt such continuity on a seasonal scale (Gründger et al., 2021). On a daily scale, tides induce
67 currents and currents disrupt continuity and hence can affect MOx, too (Steinle et al., 2015). This disruption of
68 continuity is particularly strong in the extremely dynamic inner-shelf seas where rapid changes in environmental
69 conditions can lead to rapid changes in water column dynamics.

70 The Wadden Sea, a UNESCO heritage site that consists of the largest continuous tidal flat area worldwide (14.900
71 km²), is an extremely dynamic system, with major hydrological changes occurring at seasonal to diel time scales.
72 The Wadden Sea stretches for about 500 km along the coast of the Netherlands, Germany and Denmark. Here, we
73 investigated methane dynamics in the Dutch part of the Wadden Sea, that is separated from the North Sea by five
74 barrier islands (Fig. 1). Our aim was to temporally resolve methane dynamics from an hourly to a seasonal scale
75 to determine key controls on methane dynamics and to establish a methane budget for the Dutch Waddensea



76

77 **Figure 1.** Bathymetry of the western sector of the Dutch Wadden Sea between the Marsdiep and Friesche inlet (modified from
 78 Materić et al., 2022). Tidal inlets between barrier islands facilitate water exchange with the open North Sea. The time-series
 79 station is located south of the island Terschelling (black mark; 53°19.015 N, 5°22.711 E). The offshore reference station
 80 is located 8 km north of Terschelling (white mark; 53°29.190 N, 5°21.449 E).

81

82 2 Materials and methods

83 2.1 Experimental design

84 A chain of 5 barrier islands (located 5 to 30 km offshore) shelters the Dutch Wadden Sea from waves and strong
 85 westerly winds. Between these barrier islands, large volumes of water are transported in and out the Dutch Wadden
 86 Sea with the rhythm of the tides through deep tidal inlets, such as the Marsdiep (most western point of the Dutch
 87 Wadden Sea) and the Vlie inlet (Duran-Matute et al., 2014). Our fixed mooring station (53°19.015 N, 5°22.711
 88 E) is in a branch of the Vlie inlet between the island of Terschelling and the mainland, roughly in the middle of
 89 the Dutch Wadden Sea (Fig. 1). This location was chosen as it remains submerged at low tide and lays in-between
 90 the Wadden Sea's landward and offshore termination. The water flowing by this station thus equally integrates the
 91 tidal flat area, mostly during ebb tide, as well as the inflowing North Sea water during high tide. Also, the station
 92 was relatively far away from the port of Harlingen (~ 20 km) so that a potential influence of methane rich port
 93 waters is minimized. The reference station was located 8 km north of the island Terschelling in the North Sea
 94 (53°29.190 N, 5°21.449 E).

95 Samples were recovered with the R/V Navicula during 4 sampling campaigns, respectively in winter (19 February
 96 2019 – 21 February 2019), spring (23 April 2019 – 25 April 2019), summer (22 July 2019 – 24 July 2019) and
 97 autumn (11 November 2019 – 13 November 2019). During each campaign, we conducted hourly CTD casts with
 98 discrete water sampling over a two-day period. During CTD casts, water mass properties (temperature, salinity,
 99 density) and oxygen concentrations were measured continuously using a Sea-Bird (SBE911) + conductivity-
 100 temperature-depth (CTD) system. Discrete water samples were recovered with Niskin bottles from 1 and 3 m
 101 water depth and, upon recovery, immediately sampled for subsequent analyses of water column constituents
 102 (methane concentrations, methane isotopic composition and methane oxidation rates).

103 Sediment samples were retrieved using a boxcorer, and upon recovery, subsampled with small pushcores (diameter
 104 7 cm, ~ 18 cm sediment recovery). Pushcores were subsampled for methane concentrations by taking every 2 cm
 105 5 mL of sediment that was quickly added to 60 mL glass bottles containing 30 mL of a saturated NaCl brine
 106 solution and the bottles were immediately sealed with butyl rubber stoppers. Atmospheric flask samples (250 ml)
 107 were taken hourly at ~ 10 m above the sea surface, in winter and spring. In summer and autumn, atmospheric
 108 methane concentrations were continuously measured using a cavity ringdown spectrometer (CRDS, Picarro model
 109 G2301).

110 2.2 Dissolved methane concentrations and stable isotope ratios

111 Dissolved methane concentrations were determined using a headspace (HS) technique (Green, 2005). In brief,
 112 immediately upon CTD recovery, 260 mL glass serum bottles were filled HS-free, closed with black-butyl rubber
 113 stoppers (Rubber B.V. the Netherlands) and crimp-top sealed. Next, we added a 5 mL N₂ headspace and fixed the
 114 sample with 5 mL NaOH solution (25 % w/v). HS methane concentrations of sediments and dissolved methane
 115 were measured in our home laboratories with a gas chromatograph (GC; Thermo Scientific FOCUS GC equipped
 116 with a Restek stainless steel column HS-Q 80/100 SS GEN config (length 2 m, 2 mm ID, 1/8 OD) with flame



117 ionization detection). The instrument was calibrated with a certified 100 ppm methane standard (Scott Specialty
118 Gases Netherlands B.V.).

119 Similarly, seawater aliquots were taken for methane stable carbon and hydrogen isotope measurements, but these
120 samples were fixed with 60 μl HgCl_2 (2 mM). A continuous flow isotope ratio mass spectrometry (CF-IRMS)
121 system was used to quantify D- CH_4 in the gas phase (Thermo Delta Plus XL, Thermo Fisher Scientific Inc.,
122 Germany) as described previously (Röckmann et al., 2016; Jacques et al., 2021). Isotopic values are represented
123 in the delta notation against the international reference standard VSMOW (δD). To monitor precision and
124 accuracy, sample measurements were alternated with measurements of an inhouse air standard (cross calibrated
125 against certified reference standards) containing 1975.5 ppb methane with a δD -90.81 ± 1.1 ‰. We constructed a
126 two-endmember mixing model (Mariotti et al., 1981; Jacques et al., 2021) and a Rayleigh fractionation model.
127 This was done to investigate whether enrichment of D in the residual methane was caused by MOx, which is
128 known to discriminate against heavy isotopes (Barker and Fritz, 1981; Whiticar, 1999), or by mixing with
129 comparably heavy atmospheric methane (see supplementary methods).
130

131 2.3 Methane oxidation rate measurements

132 MOx was determined by ex-situ incubations with trace amounts of ^3H -labelled methane as described previously
133 (Niemann et al., 2015). Briefly, aliquots from each Niskin bottle were filled HS-free in 20 mL glass vials in
134 triplicate, sealed with grey-bromobutyl stoppers that are known to not hamper methanotrophic activity and
135 amended with 5 μL of ^3H - CH_4/N_2 (4.5 kBq, American Radiolabeled Chemicals, USA). Samples were incubated
136 for 72 h in the dark at in situ temperature. Activities of residual C^3H_4 and the MOx product $^3\text{H}_2\text{O}$ were measured
137 by liquid scintillation counting.

138 MOx first-order rate constant (k) was determined from the fractional tracer turnover (Reeburgh, 2007):

$$139 \quad k = \frac{{}^3\text{H}_2\text{O}}{{}^3\text{H}_2\text{O} + \text{C}^3\text{H}_4} \times \frac{1}{t} \quad (2)$$

141 where t is incubation time in days. k was corrected for (negligible) tracer turnover in killed controls (KC, fixed
142 with 100 μl HgCl_2 directly after sampling) and multiplied with dissolved methane concentrations $[\text{CH}_4]$, yielding
143 MOx:

$$144 \quad \text{MOx} = (k - k_{\text{KC}}) \times [\text{CH}_4] \quad (3)$$

145

146 2.4 Diffusive fluxes of methane

147 The diffusive sea-air methane flux was calculated based on a boundary layer model that consider the relation
148 between wind, temperature and methane concentrations in the atmosphere and a well-mixed surface water layer
149 (Wanninkhof, 2014):

$$150 \quad F = (p\text{CH}_{4w} - p\text{CH}_{4a}) K_0 k_{\text{CH}_4} \quad (4)$$

151 F denotes the diffusive methane flux, $p\text{CH}_{4a}$ and $p\text{CH}_{4w}$ (in atm) are the partial pressures of methane in the air and
152 in the well-mixed surface water layer, respectively. $p\text{CH}_{4a}$ was measured with a Picarro G2301 gas concentration
153 analyser on board. $p\text{CH}_{4w}$ was determined from surface water methane concentrations (see above). K_0 is the
154 methane solubility in $\text{mol m}^{-3} \text{atm}^{-1}$ (Wiesenberg and Guinasso, 1979) and was calculated from temperature and
155 salinity obtained from corresponding CTD casts. k_{ch_4} is the methane gas transfer velocity in m d^{-1} which was
156 calculated using wind speed (U), the Schmidt number (Sc_{CH_4}) and the normalised gas transfer velocity (k_{660})
157 according to (Wanninkhof, 2014):

$$158 \quad k_{\text{CH}_4} = 0.251 U^2 \left(\frac{\text{Sc}_{\text{CH}_4}}{660} \right)^{-0.5} \quad (5)$$

159 Wind speed was measured on board at 10 m above sea level. The Schmidt number describes the ratio between
160 kinematic viscosity of water and the gas diffusion coefficient, which relates the different k -values for different
161 gases (Jähne et al., 1987; Wanninkhof, 2014).



162 **2.5 Statistical analysis**

163 A principal component analysis (PCA) was carried out to study the relationship between environmental variables
 164 and methanotrophic activity. The input variables for the PCA were temperature, salinity, density, k , MOx, and
 165 dissolved methane concentrations. Prior to running the PCA, the variables were centered and scaled. We utilized
 166 the R software and the ‘FactoMineR’ package (Lê et al., 2008) for the PCA analyses.

167

168 **3 Results**

169 **3.1 Dynamics of sea water properties**

170 Water column temperature varied between seasons and ranged from 6.3 °C to 24 °C (Fig. 2, Table 1). A clear
 171 distinction could be made between colder seasons (autumn and winter) in which temperature ranged from 6.3 °C
 172 to 9.1 °C and warmer (spring and summer) seasons where temperatures ranged from 14.2 °C to 24 °C. Water
 173 temperatures at the reference station were similar in winter (6.9 °C) but colder in spring (10.5 °C) and summer
 174 (20.3 °C) and warmer in autumn (11.8 °C) when compared to the Wadden Sea.

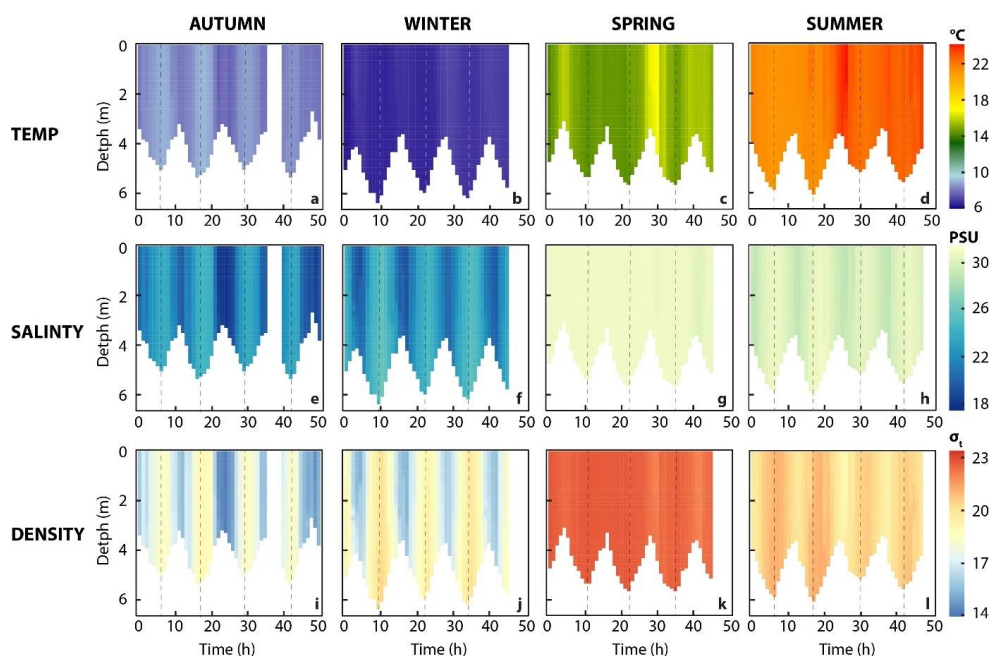
175 **Table 1.** Average seawater temperature, salinity, and density at the time-series station (central Dutch Wadden Sea) and
 176 reference station (offshore Terschelling, North Sea)

	Autumn	Winter	Spring	Summer
Temperature (°C)	8.4 ± 0.4	6.7 ± 0.2	15.0 ± 0.6	22.1 ± 0.8
Salinity (psu)	22.4 ± 1.9	23.4 ± 1.8	31.3 ± 0.2	30.6 ± 0.6
Density (σ_t)	17.4 ± 1.4	18.3 ± 1.4	23.1 ± 0.2	20.8 ± 0.6
	Autumn Ref st.	Winter Ref st.	Spring Ref st.	Summer Ref st.
Temperature (°C)	11.8 ± 0.01	6.8 ± 0.1	10.4 ± 0.12	20.0 ± 0.1
Salinity (psu)	31.3 ± 0.01	32.2 ± 0.1	31.8 ± 0.03	32.3 ± 0.03
Density (σ_t)	23.7 ± 0.01	25.2 ± 0.1	24.4 ± 0.02	22.7 ± 0.03

177

178 On a diel scale, variation in water temperature were related to the tidal phase. In winter, spring, and summer,
 179 maximum water temperatures were observed around low tide (LT, here defined as the time when we encountered
 180 the lowest water depth during CTD casts, Fig. 2). This was 7.2 °C in winter, 17.3 °C in spring and 24.1 °C in
 181 summer. Minimum water temperatures were around high tide (HT, high tide, here defined as the time when we
 182 encountered maximum water depth during CTD casts, Fig. 2). This was 6.3 °C winter, 14.2 °C in spring, and 20.9
 183 °C in summer. In autumn, this pattern was inverse with minimum water temperatures at LT (7.6 °C) and maximum
 184 at HT (9.1 °C).

185 Like temperature, salinity differed strongly between colder (18 - 27 psu) and warmer seasons (29 - 32 psu; Fig. 2,
 186 Table 1). Furthermore, salinity was higher during HT irrespective of season. Salinity levels at the reference station
 187 in the North Sea were stable (31.3 – 32.3 psu) without obvious diel and seasonal fluctuations. Changes in density
 188 were caused by salinity rather than temperature during all four seasons, with one exception in spring: after 28
 189 hours of the time series, salinity remained stable, but water temperatures decreased which lowered water density.



190

191 **Figure 2.** Properties of sea water. (a-d) Spatiotemporal distribution of temperature, (e-h) salinity and (i-l) density. Dashed
192 line indicates high tide.

193 3.2 Methane dynamics

194 3.2.1 Methane concentrations in the water column and in sediments

195 Water column methane concentrations showed a high degree of variability and were clearly distinguishable
196 between the colder and warmer seasons (Fig. 3A-D, Table 2). We found a significant difference in average methane
197 concentrations between 1 m (16.0 nM) and 3 m (17.6 nM) water depth in winter ($p \leq 0.007$, Welch's t-test). In
198 autumn, methane concentrations were also lower at 1 m (15.5 nM) than at 3 m (16.2 nM) water depth, but the
199 difference was not significant. However, it is noteworthy that the methane concentrations at the beginning of the
200 time-series were around 35 nM and rapidly decreased to values below 15 nM within one day. During warmer
201 seasons, average methane concentrations were similar at the surface and in deeper waters, i.e. 40.9 nM (1 m) and
202 41.3 nM (3 m) in spring and 69.2 nM (1 m) and 69.4 (3 m) in summer. Methane concentrations at our reference
203 station were ~ 3 nM in winter, spring, and autumn and ~ 6 nM in summer and thus far lower when compared to
204 the Wadden Sea.

205 On a diel scale, methane concentrations varied during all seasons, roughly matching the tidal regime. In spring at
206 LT, depth-averaged methane concentrations were 42.6 nM, but decreased by ~ 25 % to 34.2 nM at HT. This pattern
207 also occurred in autumn where methane concentrations decreased by 21 % from 17.4 nM at LT to 14.4 nM at HT.
208 In winter (14.7 nM at LT and 14.3 nM at HT) and summer (72.5 nM at LT and 71.3 nM at HT), the difference
209 between LT and HT was smaller (Table 2).

210 Sediment methane concentrations increased with depth during all seasons (Fig. S1 in the Supplement).
211 Concentrations were similar in autumn (0.5 – 2.2 μM), winter (0.4 - 0.6 μM) and spring (0.5 - 0.9 μM) but in
212 summer, we found highly elevated sediment methane concentrations ranging from 3.6 to 18.7 μM . The high
213 concentrations in sediments during the summer season are in line with an increase in dissolved methane
214 concentrations in the water column.

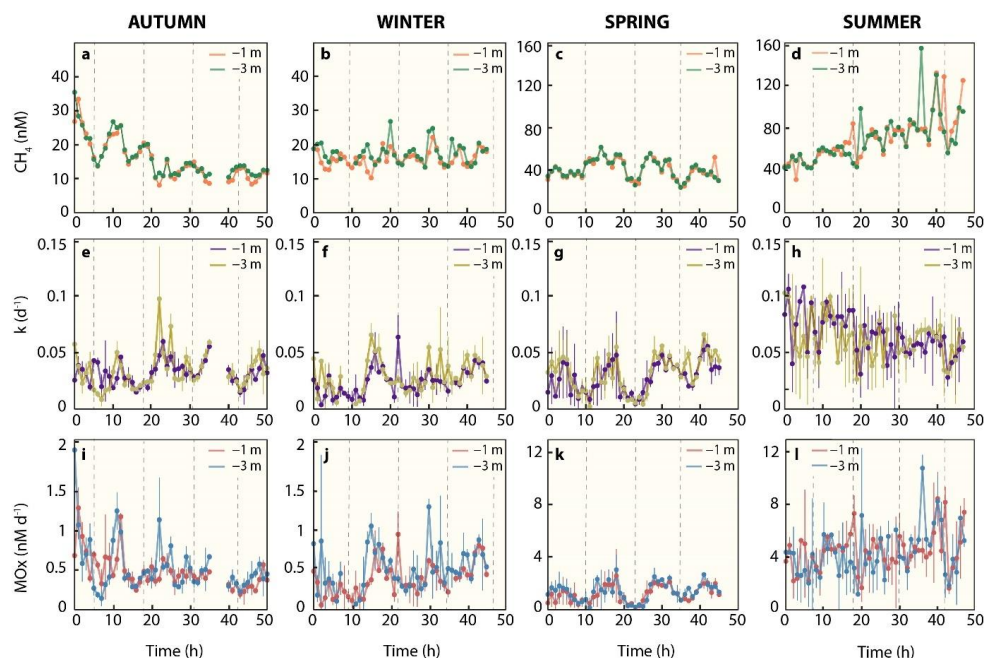
215



216 **Table 2. Methane dynamics in the Dutch Wadden Sea.** Average and standard deviation of methane concentrations, k , MOx
 217 and $\delta D-CH_4$ during four seasons in 2019. Values represent averages for 1 and 3 m water depth (averaged over the two-day time
 218 series recorded for each season) as well as for low and high tide only (averaged over depth). LT = minimal water depth during
 219 CTD casts, HT = maximum water depth during CTD cast. Average wind speed and methane efflux to the atmosphere are
 220 averaged over the two-day time series recorded for each season. ns = not sampled.
 221

	Autumn	Winter	Spring	Summer
Methane concentration (nM)				
1 m water depth	15.5 ± 5.8	16.0 ± 2.4	40.9 ± 9.2	69.2 ± 21.4
3 m water depth	16.2 ± 5.7	17.6 ± 3.0	41.3 ± 8.9	69.4 ± 22.4
Low tide	17.4 ± 9.7	14.7 ± 2.1	42.6 ± 6.9	72.5 ± 36.1
High tide	14.4 ± 1.6	14.3 ± 0.6	34.2 ± 10.7	71.3 ± 27.4
Reference station	3.3	3.1	3.7	6.6
k (d⁻¹)				
1 m water depth	0.03 ± 0.01	0.02 ± 0.01	0.03 ± 0.01	0.07 ± 0.02
3 m water depth	0.03 ± 0.02	0.03 ± 0.01	0.03 ± 0.02	0.06 ± 0.02
Low tide	0.05 ± 0.01	0.03 ± 0.01	0.05 ± 0.01	0.08 ± 0.02
High tide	0.03 ± 0.01	0.03 ± 0.02	0.02 ± 0.01	0.06 ± 0.02
Reference station	0.01	0.0004	0.02	0.04
MOx (nM d⁻¹)				
1 m water depth	0.48 ± 0.22	0.39 ± 0.21	1.16 ± 0.61	4.41 ± 1.49
3 m water depth	0.54 ± 0.34	0.52 ± 0.27	1.33 ± 0.71	4.33 ± 1.84
Low tide	1.05 ± 0.48	0.47 ± 0.24	2.02 ± 0.42	5.24 ± 2.33
High tide	0.50 ± 0.16	0.43 ± 0.31	0.59 ± 0.19	4.23 ± 2.13
Reference station	0.03	0.001	0.07	0.23
$\delta D-CH_4$ (‰)				
1 m water depth	-219 ± 31	ns	ns	-250 ± 17
3 m water depth	-224 ± 27	ns	ns	-250 ± 14
Low tide	-208 ± 41	ns	ns	-227 ± 1
High tide	-227 ± 13	ns	ns	-265 ± 3
Methane sea-air flux ($\mu\text{mol m}^{-2} \text{d}^{-1}$)				
Wind speed (m s ⁻¹)	8.0 ± 2.1	8.3 ± 1.4	7.9 ± 2.7	3.8 ± 1.6
Methane flux	40.2 ± 28.1	38.7 ± 14	144.8 ± 98	72.9 ± 52
Atmosphere conc. (ppm)	2.0 ± 0.03	2.12 ± 0.19	2.02 ± 0.15	2.14 ± 0.15

222



223

224 **Figure 3.** Methane dynamics. (a-d) Dissolved methane concentration, (e-d) first-order rate constant, (i-l) methane oxidation
 225 rates. Note that for dissolved methane concentrations in colder seasons, autumn and winter, the y-axis differs from warmer
 226 seasons, spring, and summer. Dashed line indicates high tide.

227 3.2.2 Methane oxidation rates

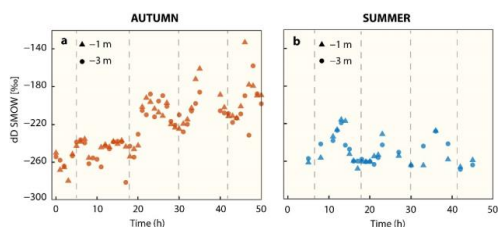
228 Similar to methane concentrations, we observed strong seasonal differences in MOx (Fig. 3I-L, Table 2). Depth-
 229 averaged MOx in spring (1.2 nM d^{-1}) and summer (4.4 nM d^{-1}) was ~ 3 and ~ 9 – fold higher than in winter (0.5
 230 nM d^{-1}) and autumn (0.5 nM d^{-1}). MOx at 1 m and 3 m water depth statistically differed from each other in winter
 231 ($p \leq 0.01$, Welch’s t-test), but not in spring, summer, and autumn. MOx at the reference station was $< 5\%$ of MOx
 232 in the Wadden Sea, with maxima found in summer (0.2 nM d^{-1}).

233 On a diel scale, MOx showed fluctuations during all seasons. In general, depth-averaged MOx was higher during
 234 LT compared to HT. In autumn average MOx at LT (0.79 nM d^{-1}) was about 2 – fold higher and significant different
 235 from MOx at HT (0.38 nM d^{-1} , $p \leq 0.03$, Welch’s t-test).

236 In winter, the difference between MOx at LT (0.47 nM d^{-1}) and HT (0.43 nM d^{-1}) was small. In spring, depth-
 237 averaged MOx at LT (2.02 nM d^{-1}) was about 4 – fold and significantly ($p \leq 6.4 \times 10^{-6}$, Welch’s t-test) higher than
 238 during HT (0.58 nM d^{-1}). In summer, MOx was high at both, LT (5.2 nM d^{-1}) and HT (5.4 nM d^{-1}). Similarly, k
 239 was substantial higher (16 – 63 %) at LT than HT in all seasons (Fig. 3E-H, Table 2). In fact, the difference in
 240 depth-averaged k between LT and HT was significant in autumn ($p \leq 0.003$, Welch’s t-test) and spring ($p \leq 6 \times$
 241 10^{-5} , Welch’s t-test, Table S1 in the Supplement).

242 3.2.3 Stable hydrogen isotope signatures

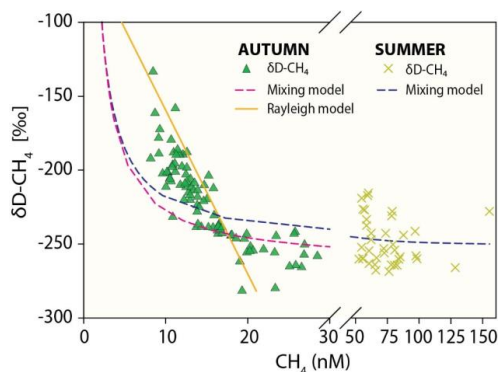
243 The stable hydrogen isotope composition of dissolved methane was only measured in autumn and summer (Fig.
 244 4, Table 2). In autumn, average $\delta\text{D-CH}_4$ over the entire time-series was -219‰ at 1 m water depth and -224‰
 245 at 3 m water depth, but there was a generally strong trend towards higher $\delta\text{D-CH}_4$ values over the two-day period
 246 from about -260‰ to about -180‰ . In summer the mean $\delta\text{D-CH}_4$ values were homogenous throughout the water
 247 column (-250‰) and generally lower than in autumn. Except for the first full tidal cycle in autumn, the results
 248 showed a tidal imprint on $\delta\text{D-CH}_4$ values with higher $\delta\text{D-CH}_4$ values at LT and lower values at HT independent
 249 of depth and season (Fig. 4).



250

251 **Figure 4.** Progression of $\delta\text{D-CH}_4$ signatures in (a) autumn and (b) summer at 1 m and 3 m water depth. Vertical dashed line
252 indicates high tide.

253 In addition to tidal patterns, the $\delta\text{D-CH}_4$ values in autumn were substantially higher at lower methane
254 concentrations (< 21 nM, Fig. 5). Linear mixing alone of (i) well-mixed surface waters in equilibrium with
255 atmospheric methane and (ii) the maximum methane concentration in the water column, both concentrations with
256 their associated isotopic signatures, would result in concentration/isotope data as depicted by the mixing lines in
257 Fig. 5. Results in autumn clearly deviated from this mixing line at low methane concentrations. On the other hand,
258 the open system Rayleigh fractionation model that we ran for low methane concentration in autumn yielded an ϵ -
259 value of -97 ‰ and matched the steep rise in $\delta\text{D-CH}_4$ with decreasing methane concentration much better. This
260 directly indicates that MOX is the dominant mechanism driving $\delta\text{D-CH}_4$ to higher values at low concentrations.



261

262 **Figure 5.** Methane concentration versus $\delta\text{D-CH}_4$ - mixing and oxidative removal in autumn and summer. Dashed lines show
263 methane concentration/isotope dynamics determined with a two-endmember mixing model considering (i) well-mixed Wadden
264 Sea surface waters and (ii) methane charged waters as endmembers. Methane concentration and stable hydrogen isotope
265 composition following oxidative removal according to a Rayleigh model for low methane concentrations are depicted as a solid
266 line. Samples with methane concentrations < 21 nM ($\delta\text{D-CH}_4 = \sim -217$ ‰) in autumn and < 61 nM ($\delta\text{D-CH}_4 = \sim -244$ ‰) in
267 summer were defined as the methane source signal and thus starting point of the Rayleigh fractionation model. The apparent
268 isotope enrichment (ϵ see also Fig. S2 in the Supplement) was -97 ‰ in autumn. Neither the mixing nor the Rayleigh model
269 are well constrained for $\delta\text{D-CH}_4$ in summer; the mixing line is thus only shown for comparison and ϵ could not be calculated.

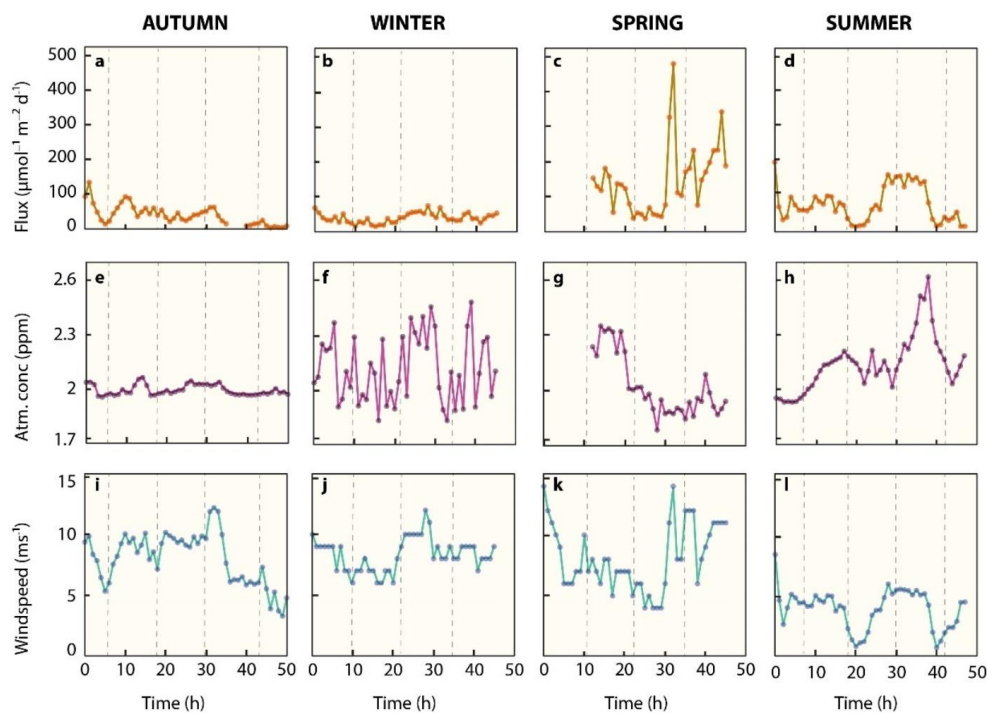
270 3.2.4 Diffusive efflux to the atmosphere

271 The water column in the Wadden Sea was consistently methane supersaturated (> 8 nM) with respect to
272 atmospheric equilibrium (~ 2.6 nM) during all sampling campaigns (Fig. 3, Table 2), which indicates a continuous
273 release of methane from the water to the atmosphere throughout the measurement series. Atmospheric
274 concentrations were similar ranging from 1.8 to 2.6 ppm, with relatively constant concentrations in autumn and
275 more erratic concentrations in winter, spring, and summer (Fig. 6e-h, Table 2). Noteworthy is the sharp increase
276 of atmospheric methane from 2 to 2.6 ppm between 29 and 38 hours in summer before decreasing again to 2 ppm.

277 Windspeeds in autumn, winter, and spring were relatively high (typically > 5 ms^{-1}) when compared to calmer
278 conditions in summertime (typically < 5 ms^{-1} , Fig. 6i-l, Table 2). As a result of the strong but variable wind forcing,
279 diffusive methane fluxes fluctuated in magnitude within, and between season (Fig. 6a-d, Table 2). Average
280 diffusive fluxes in autumn and winter were with < 40 $\mu\text{mol m}^{-2} \text{d}^{-1}$ about 4 – fold lower than in spring and 2 – fold
281 lower than in summer. Maximum efflux (479 $\mu\text{mol m}^{-2} \text{d}^{-1}$) in spring occurred after the wind velocity increased



282 rapidly from 6 m s^{-1} to 14 m s^{-1} within two hours and methane concentrations slightly increased from 38 nM to 45
283 nM.



284

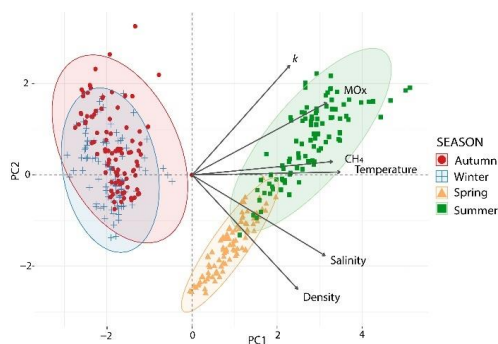
285 **Figure 6.** Diffusive methane flux. (a-d) Sea surface atmosphere methane fluxes, (e-h) Seasonal atmospheric methane
286 concentrations, (i-l) local wind speed. Vertical dashed lines indicate high tide.

287



288 **3.3 Statistical Analysis**

289 To study the relationship between environmental variables and methanotrophic activity, we conducted a Principal
 290 Component Analysis (PCA). The outcome explained 92 % of the data variability on the first two components (Fig.
 291 7, Table S2 in the Supplements). The main gradient (PC1: 69 %) showed a contrast between autumn/winter and
 292 summer and spring. Temperature, salinity, methane concentrations and MOx peaked in summer and spring, while
 293 lower values were measured in winter/autumn. The relatively small ellipse in spring indicates that samples show
 294 more similarity than in other seasons. The second gradient distinguished the summer from the spring samples
 295 based on higher *k* and density in the latter (PC2: 23 %).



296

297 **Figure 7.** Principal Component Analysis (PCA) of environmental conditions across seasons in the Dutch Wadden Sea. Biplot
 298 of a PCA of the explanatory variables as vectors (in black) and observations (marks) of each season on the first (x-axis, PC1)
 299 and second principal component (y-axis, PC2). Coloured concentration ellipses (size determined by a 0.95-probability level)
 300 show the observations grouped by season. The magnitude of the vectors (line length) shows the strength of their contribution
 301 to the PCs. Vectors pointing in similar directions indicate positively correlated variables and vectors at angles > 90° indicate
 302 no correlation.

303 **4 Discussion**

304 The Wadden Sea is a highly productive ecosystem (Philippart et al., 2009) where the decay of organic matter
 305 supports high rates of methanogenesis in sediments (Røy et al., 2008; Wu et al., 2015), which in return leads to
 306 high methane concentrations in the Wadden Sea's water column (Grunwald et al., 2007; Grunwald et al., 2009).
 307 Little knowledge, however, exists on the variability of methane dynamics on short time scales of hours to days or
 308 between seasons and the underlying controls on this variability. Here, we measured water column methane
 309 concentrations, methane oxidation and the oceanographic regime as well as atmospheric methane mixing ratios
 310 and wind velocity in the Dutch sector of the Wadden Sea for two days during four consecutive seasons in 2019.

311 **4.1 Water column properties**

312 In general, we found a clear distinction between colder (autumn and winter) and warmer (spring and summer)
 313 seasons (Figs. 2, 7). North Sea waters with incoming tide, flow through tidal inlets that in turn branch into
 314 successively smaller tidal creeks in which water-flow direction alternates with the tidal phase. This then led to
 315 increasing water temperatures in autumn but decreasing water temperatures in winter. The high temperature of
 316 Wadden Sea waters during incoming tide in autumn can be explained by the fact that the shallow Wadden Sea
 317 cools rapidly once the summer is over, while the North Sea's large water volume takes longer to cool down.

318 Salinity levels were on average lower in colder seasons compared to warmer seasons, likely because land runoff
 319 and ground water discharge are typically higher in autumn and winter because of the overall higher precipitation
 320 levels during the cold seasons (Van Aken, 2008). A higher level of freshwater inflow from land was also evident
 321 from the rapidly dropping salinity levels during falling and LT in autumn and winter (Fig. 2). This freshening
 322 effect is amplified at times when the Dutch Ministry of Infrastructure and Water management (Rijkswaterstaat)
 323 opens water gates to discharge excess water from lake IJssel (Fig. 1), which occurs more often in colder seasons
 324 due to increased input of precipitation, groundwater discharge as well as surface and riverine discharge to the lake.
 325 During the warmer and dryer seasons, water gates are mostly kept closed to ensure that the lake's water level stays
 326 high. However, freshwater inflow into the Wadden Sea was evident during all seasons because incoming North
 327 Sea water generally increased salinity levels at HT independent of sampling time.



328 **4.2 Differences in methane concentrations and isotopic signatures on time scales of seasons**

329 Sediment and water column methane concentrations were highly elevated in summer (Figs. 3, S1 in the
330 Supplement and Table 2). In fact, average sediment methane concentrations increased 17 – fold in summer
331 compared to spring two months earlier. This increase is probably related to the remineralization of the spring
332 phytoplankton bloom that takes place in the months of April and May (Philippart et al., 2009) leading to elevated
333 rates of methanogenesis in anaerobic sediments (Beck and Brumsack, 2012). A time lag of one to two months
334 between the peak of the spring bloom and methane release from sediments was also observed in the Baltic Sea
335 (Bange et al., 2010). In addition to elevated inputs of organic matter, increasing water temperatures towards
336 summer further enhances microbial methanogenesis in sediments (Yvon-Durocher et al., 2014). We indeed
337 observed lower methane concentrations in autumn and winter compared to spring and summer, which is most
338 likely related to both reduced organic matter input and colder temperatures. It has to be noted that the sediment
339 methane concentrations presented here are comparably low as sediment methane concentrations close to saturation
340 levels were previously found at other locations in Wadden Sea sediments (Røy et al., 2008; Wu et al., 2015). We
341 did not measure sulphate concentrations, but the methane profiles indicate that we only reached the upper part of
342 the methane-sulphate transition zone below of which methanogenesis proceeds. Also, sediment methane
343 concentrations can be variable on spatial scales of metres. Depending on the hydrographic regime, the methane-
344 sulphate transition zone can be metres below the tidal flat sediments (Wu et al., 2015), but pore water flow can
345 also transport reduced compounds such as sulphide and methane to the sediment surface (Røy et al., 2008).

346 Methane release from sediments and the relatively low wind speed (and thus relatively low forcing to drive
347 diffusive efflux) in summer led to charging of the water column with methane. MOx discriminates against
348 isotopically heavy methane and thus causes an isotopic enrichment of residual methane. This isotopic
349 discrimination effect manifests more pronouncedly at low methane concentrations. Indeed, we found more
350 pronounced MOx induced isotopic discrimination effects in autumn at low methane concentrations (< 21 nM). At
351 higher methane concentrations (> 21 nM) values were more depleted and were comparable to summer $\delta\text{D-CH}_4$
352 values. We relate the $\delta\text{D-CH}_4$ values (~ -217 ‰ in autumn and ~ -244 ‰ in summer) at higher methane
353 concentrations (> 21 nM in autumn and > 61 nM in summer) to the $\delta\text{D-CH}_4$ source signal (Fig. 4A, 5). At these
354 concentrations, the isotope effect imposed by MOx is masked by the high background methane and/or is
355 overprinted by methane entering the water column from sediments.

356 **4.3 Differences in MOx on seasonal time scales**

357 The activity of MOBs in the water column is determined by the availability of methane, oxygen, nutrients, and the
358 size of the standing stock of the MOB community (Reeburgh, 2007; Crespo-Medina et al., 2014; Steinle et al.,
359 2015). The Wadden Sea water column is a nutrient rich and typically oxygenated environment, we hence argue
360 that nutrient and O₂ availability are not a limiting factor for MOB activity. However, MOBs in the Wadden Sea
361 need to cope with high fluctuations in temperature, salinity, and methane availability (see above). We did not
362 measure the size of the MOB community; nevertheless, it seems likely that the highly variable water column
363 properties with admixture of different water masses and resuspension of particles effects the standing stock of the
364 MOB community and/or its activity.

365 Previous studies showed that elevated salinity often led to an immediate decrease in MOx in terrestrial/lacustrine
366 systems (Ho et al., 2018; Zhang et al., 2023). Likewise, marine methanotrophs seem to function best at salinity
367 levels of > 20 psu (Osudar et al., 2017), while a sudden decrease in salinity can strongly inhibit MOx (Hirayama
368 et al., 2013; Tavormina et al., 2015). This begs the question if waters, with rapidly changing salinity levels such
369 as the Wadden Sea, are environments that are rather not conducive for MOx, in particular in colder months where
370 salinity levels may drop to ~ 20 psu because of elevated freshwater influx (see above). While MOx was indeed
371 lower in autumn and winter, the relative decrease in MOx was moderate in comparison to the previous literature
372 findings (Osudar et al., 2017; Zhang et al., 2023). Also, autumn and winter are colder and defined by lower methane
373 levels, which likely reduces MOx further. Across seasons, the PCA (Fig. 7), and Pearson correlation coefficients
374 of pairs of variables (Fig. S3 in the Supplement) indicated that MOx (or *k*) and salinity (or density) are not or only
375 weakly correlated. The Wadden Sea thus seems to host a euryhaline MOB community that contrast with MOB
376 communities from terrestrial/lacustrine (Zhang et al., 2023) and oceanic origin (Osudar et al., 2015), which seem
377 less able to cope with varying salinity levels.

378 Sediments and the water column in the Wadden Sea are increasingly fuelled with methane when ambient
379 temperatures rise. The higher availability of methane could then enhance methanotrophic activity (Reeburgh,
380 2007). Indeed, we found a seasonal imprint with highest MOx levels in summer that were 3-fold higher than those



381 observed in spring, 9-fold higher than in autumn and 10-fold higher than in winter (Table 2). A correlation between
382 methane, temperature and MO_x was also apparent from the PCA (Figs. 7, S3 in the Supplement). We note that not
383 only MO_x, but also the first order rate constant k was stimulated by higher methane concentrations (MO_x is a
384 function of k and [CH₄], see eq. 3) and temperature. A positive effect of methane on MO_x and k is often associated
385 with changes in methane concentrations over several orders of magnitude (Crespo-Medina et al., 2014; James et
386 al., 2016). Here we found that k doubled in summer compared to spring, while methane concentrations were only
387 30 nM higher, i.e., 1.7-fold. This suggests that a combination of methane availability and temperature determined
388 k in our study. I.e., the MOB_s may have been stimulated on the enzymatic level. However, the fact that k remained
389 stable in colder seasons with low water temperatures, suggest that additional factors, likely MOB community size
390 (Steinle et al., 2015), might play a more important role in maintaining k . For example, MOB_s from sediments can
391 be resuspended into the water column due to tidal currents, or transported from sediments to the water-column
392 with bubbles as has been found at other cold seeps (Steinle et al., 2016; Jordan et al., 2020; Jordan et al., 2021).
393 Resuspension could thus be a key driver of the Wadden Sea water column MOB communities, with major
394 consequences for maintaining a microbial filter under less favourable conditions.

395 **4.4 Methane dynamics on times scales of hours to days.**

396 Strong hydraulic dynamics are an important characteristic of the Dutch Wadden Sea, with tidal currents
397 interchanging a large water volume with the North Sea twice per day (Gräwe et al., 2016). With the change in tidal
398 phase, the hydrostatic pressure changes rapidly with water depth, which triggers porewater flow (tidal pumping,
399 Røy et al., 2008) but may also trigger expansion and ebullition of gas bubbles (Schmale et al., 2015; Jordan
400 et al., 2020). Similar effects are caused by tidal currents flowing over bathymetric features, which triggers pore water
401 flow, too, and additionally resuspends sediments and MOB_s into the water column (Bussmann, 2005; Abril et al.,
402 2007; Røy et al., 2008). On the other hand, incoming water from the open North Sea contains relatively low
403 amounts of methane (<6 nM as measured at our reference station), hence, this will dilute the Dutch Wadden Sea's
404 methane content, and outflowing water will export methane from the Dutch Wadden Sea main water body.

405 Temporal patterns of methane concentration and MO_x indeed correlated well with tidal oscillation (Figs. 3, S1 in
406 the Supplements, Table 2). Independent of the seasons, methane concentrations and MO_x were elevated at LT.
407 The tidal effect seemed most pronounced in spring where at LT, methane concentrations (1.3 – fold), k (2.5 – fold)
408 and MO_x (4 – fold) were higher than at HT, independent of depth. We found it surprising that, just like methane
409 concentrations, k also was substantially higher during LT compared to HT independent of seasons and despite an
410 overall lower salinity at low tide (Figs. 3, S1 in the Supplement, Table 2). To the best of our knowledge, this has
411 not been described before. It seems unlikely that the MOB community substantially grew or that the velocity of
412 the MOB's metabolism increased/decreased in a time frame of a few hours. We rather argue that the observed
413 oscillation is caused by a likewise oscillation of shear force and hydrostatic pressure, leading to resuspension of
414 MOB_s from sediments as well as elevated release of methane from the sea floor.

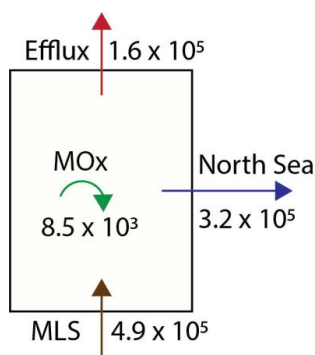
415 Grunwald et al. (2007 and 2009) conducted time-series measurements in the German sector of the Wadden Sea
416 near the island of Spiekeroog. There, absolute methane concentrations were ~ 3 – fold higher in spring and summer
417 and ~ 15 – fold higher in winter when compared to our study. This might be related to local factors, for example
418 the vicinity of the estuaries of the rivers Eems and more importantly Weser close by Spiekeroog, which increase
419 the background methane concentrations in this sector of the Wadden Sea. Like in our study, Grunwald et al. (2007,
420 2009) also reported on a strong influence of tides, with highest methane concentrations at low tide, probably related
421 to tidal pumping, while inflowing waters showed concentrations typical for the open North Sea in the German
422 Bight. The temporal aspects and processes determining methane dynamics discussed in our work are thus not a
423 local feature but applicable to the entire Wadden Sea and likely to other mud flat areas influenced by tides, too.

424 **4.5 Methane emissions from the Dutch Wadden Sea**

425 Surface waters were supersaturated in methane with respect to the atmospheric equilibrium during all seasons; the
426 Wadden Sea is consequently a constant source of methane to the atmosphere. Just as for dissolved methane
427 concentrations and MO_x, methane efflux to the atmosphere was higher during warmer seasons compared to colder
428 seasons. This was primarily driven by methane concentrations rather than wind velocity: wind speeds were similar
429 in autumn, winter, and spring, but 2-fold higher methane concentrations in spring translate to a 4-fold higher sea-
430 air flux when compared to autumn and winter. In summer, meteorological conditions were dominated by a heat
431 wave with extremely low wind speeds. This resulted in a comparably low methane efflux to the atmosphere
432 (though still higher than during the colder seasons) leading to an accumulation of methane in the water column.
433 Previously described diffusive methane fluxes at coastal systems vary over several orders of magnitude and appear



434 site specific. At the Baltic sea coast, fluxes of up to $15 \mu\text{mol m}^{-2} \text{d}^{-1}$ were reported (Bange et al., 2010; Steinle et
 435 al., 2017), while in arctic shelf seas, diffusive fluxes of up to $240 \mu\text{mol m}^{-2} \text{d}^{-1}$ were found (Thornton et al., 2016).
 436 In comparison, estuarine research along the European Atlantic coast found a median flux of $130 \mu\text{mol m}^{-2} \text{d}^{-1}$
 437 (Middelburg et al., 2002), which is comparable to the fluxes that we found in the Dutch Wadden Sea (~ 39 to 145
 438 $\mu\text{mol m}^{-2} \text{d}^{-1}$).



439

440 **Figure 8.** Methane budget for the Dutch Wadden Sea is calculated based on values for the Wadden Sea's geometry, tidal
 441 displacement volume, and biogeochemical parameters as discussed in the text. MLS stands for methane liberation from
 442 sediments. All values are presented as $\text{mol CH}_4 \text{d}^{-1}$.

443 Towards a roughly estimated methane budget for Dutch Wadden Sea, we combined our diffusive flux, MOx and
 444 methane concentration data (Fig 8.) as well as estimates of the Wadden Sea water volume and tidal prism. Our
 445 flux estimates (Table 2) translate to an annual average sea surface-atmosphere flux of $74 \mu\text{mol m}^{-2} \text{d}^{-1}$.
 446 Extrapolating this to the area of Dutch sector of the Wadden Sea ($\sim 2200 \text{ km}^2$; (Materić et al., 2022) implies that
 447 $1.6 \times 10^5 \text{ mol CH}_4 \text{d}^{-1}$ escapes from the Dutch Wadden Sea to the atmosphere (Table 2). The average water volume
 448 of the Dutch Wadden Sea is about 5.15 km^3 (Materić et al., 2022); hence the annual average of 1.7 nM d^{-1} of MOx
 449 translates to $0.09 \times 10^5 \text{ mol CH}_4 \text{d}^{-1}$ that is oxidized in the water column by MOBs. In addition to atmospheric
 450 efflux and microbial consumption, methane rich waters are also flushed into the North Sea. To estimate this, we
 451 simplified that the total tidal prism of 4.5 km^3 (Gräwe et al., 2016) is an approximation of the net amount of water
 452 that leaves the Wadden Sea during LT. With respect to our measured mean methane concentration (36.8 nM),
 453 about $1.6 \times 10^5 \text{ mol}$ of methane are thus flushed towards the North Sea twice daily, i.e., $3.2 \times 10^5 \text{ mol}$ per day. A
 454 large uncertainty in this calculation is caused by the delay of ~ 3 hours in tidal phases between the Western and
 455 Eastern part of the Dutch Wadden Sea. In other words, methane-rich waters are flowing out of the tidal inlet in the
 456 West can be entrained in the current that starts flowing back into the Wadden Sea at eastern tidal inlets. Therefore,
 457 the net loss of methane to the Wadden Sea is probably lower than described above. Still, data from our reference
 458 station show only slightly oversaturated methane concentrations ($< 6 \text{ nM}$) suggesting that the amount of methane
 459 flowing back into the Wadden Sea is rather low. A similar observation was found during a tidal inlet study in the
 460 German Wadden Sea (Grunwald et al., 2009). Though overall methane concentrations were higher, methane
 461 concentrations in North Sea waters flowing into the Wadden Sea were 60 % lower compared to waters flowing
 462 out of the Wadden Sea at low tide. Excluding allochthonous methane sources (for example methane influx with
 463 freshwater from Lake IJssel), the Dutch Wadden Sea's methane budget must be supported by a total rate of
 464 methanogenesis that at least equals the sum of methane efflux to the atmosphere, water column methanotrophy
 465 and methane outflow to the North Sea; together these amount to $4.9 \times 10^5 \text{ mol d}^{-1}$. This is comparable to
 466 methanogenesis rates in the Eckernförde Bay in the Baltic Sea in the Baltic Sea (Maltby et al., 2018). Note that
 467 this accounts for the amount of methane liberated from sediments, while it neglects methane oxidation in sediments
 468 (dominantly anaerobic oxidation of methane), which can retain a substantial fraction of methane in sediments
 469 (Reeburgh, 2007). Hence, the total rate of methanogenesis in the Wadden Sea is consequently much higher.

470 Taken all methane export terms/sinks considered together (MOx, efflux and tidal displacement amounting to 4.9
 471 $\times 10^5 \text{ mol d}^{-1}$), MOx reduces roughly 2 % of the Wadden Sea's methane budget, while about $1/3^{\text{rd}}$ of methane
 472 escapes to the atmosphere and the remaining $\sim 2/3^{\text{rd}}$ is flushed into the North Sea (where it may be further oxidised
 473 and/or released to the atmosphere). The effect of MOx on the methane budget is low when compared to the global
 474 ocean, where an estimated >90 % of water column methane is consumed by MOx (Reeburgh, 2007). As the
 475 Wadden Sea is very shallow, liberation of methane from sediments to the atmosphere is fast; in other words, MOBs



476 have a very limited time to consume methane released from the sediments before it is liberated to the atmosphere
477 or flushed with tides to the North Sea. Weber et al. (2019) estimated that coastal systems globally contribute
478 between 0.8 and 3.8 Tg y⁻¹ of methane to the atmospheric budget. We found a total annual sea-air flux from the
479 Dutch sector of the Wadden Sea (2200 km²) of ~ 0.001 Tg y⁻¹. The Dutch sector of the Wadden Sea alone may
480 thus already account for 0.03 % to 0.1 % of the global methane emission from the global coastal ocean.

481 **5 Summary and conclusion.**

482 Our work revealed substantial variations in methane dynamics when comparing colder and warmer seasons; in
483 warmer seasons, methane concentrations, efflux and MO_x were higher compared to colder seasons. Still during
484 colder seasons waters were continuously supersaturated with methane and higher wind speeds in these seasons led
485 to substantial amounts of methane released to the atmosphere. We show that tidal dynamics are a key control for
486 methanotrophic activity and methane distribution. Although changing water column properties and methane
487 concentrations do not provide continuity, the capacity of the microbial methane filter is seemingly stable, with an
488 active MOB community even under unfavourable conditions. Nevertheless, MO_x only consumes a minor fraction
489 of the methane inventory of the highly dynamic Wadden Sea, while most is or liberated to the atmosphere and
490 flushed out with tidal currents into the neighbouring North Sea. It appears likely that the contribution of the
491 Wadden Sea to the global atmospheric methane budget will alter in the future due to global warming, and changes
492 in nutrient availability and more frequently occurring storm events. Our results finally highlight the importance of
493 repeated high frequency sampling strategies in dynamic coastal waters to resolve temporal patterns on diel and
494 seasonal scales.

495 *Data availability.* All data will be archived and made publicly available in the data base DAS (Data Archive
496 System, www.nioz.nl/en/research/dataportal/das).

497
498 The supplement related to this article is available online.

499
500 *Author contributions.* The study was designed by Tim de Groot, Thomas Röckmann, and Helge Niemann. On-
501 board sampling was performed by Tim de Groot, Anne Mol, Katherine Mesdag, Julia Engelmann, Pierre Ramond,
502 and Helge Niemann. Further geochemical analysis was conducted by Tim de Groot, Anne Mol, Katherine Mesdag,
503 and Rachel Ndhlovu. Microbial rates were measured by Tim de Groot and Anne Mol. Statistical analysis was
504 carried out by Tim de Groot and Pierre Ramond. Helge Niemann supervised the research project. The manuscript
505 was prepared by Tim de Groot with input from all authors.

506 *Competing interests.* The authors disclose that at least one of the (co-)authors holds a position on the editorial
507 board of Biogeosciences.

508
509 *Acknowledgements.* Our gratitude goes to the captain and crew of R/V Navicula, as well as the staff of the
510 geochemical, radioisotope, and atmospheric laboratories at NIOZ and IMAU, for their exceptional support. We
511 would also like to extend our appreciation to Eric Wagemakers for regularly calibrating the CTD.

512 **References**

- 513 Abril, G., Commarieu, M.-V., and Guérin, F.: Enhanced methane oxidation in an estuarine turbidity maximum,
514 *Limnology and Oceanography*, 52, 470-475, <https://doi.org/10.4319/lo.2007.52.1.0470>, 2007.
- 515 Bange, H. W., Bartell, U. H., Rapsomanikis, S., and Andreae, M. O.: Methane in the Baltic and North Seas and a
516 reassessment of the marine emissions of methane, *Global Biogeochemical Cycles*, 8, 465-480,
517 <https://doi.org/10.1029/94GB02181>, 1994.
- 518 Bange, H. W., Bergmann, K., Hansen, H. P., Kock, A., Koppe, R., Malien, F., and Ostrau, C.: Dissolved methane
519 during hypoxic events at the Boknis Eck time series station (Eckernförde Bay, SW Baltic Sea), *Biogeosciences*,
520 7, 1279-1284, 10.5194/bg-7-1279-2010, 2010.
- 521 Barker, J. F. and Fritz, P.: Carbon isotope fractionation during microbial methane oxidation, *Nature*, 293, 289-291,
522 10.1038/293289a0, 1981.
- 523 Beck, M. and Brumsack, H.-J.: Biogeochemical cycles in sediment and water column of the Wadden Sea: The
524 example Spiekeroog Island in a regional context, *Ocean & Coastal Management*, 68, 102-113,
525 10.1016/j.ocecoaman.2012.05.026, 2012.
- 526 Boetius, A. and Wenzhöfer, F.: Seafloor oxygen consumption fuelled by methane from cold seeps, *Nature*
527 *Geoscience*, 6, 725-734, 10.1038/ngeo1926, 2013.
- 528 Bussmann, I.: Methane Release through Resuspension of Littoral Sediment, *Biogeochemistry*, 74, 283-302,
529 10.1007/s10533-004-2223-2, 2005.



- 530 Canadell, J. G., Monteiro, P. M. S., Costa, M. H., Cotrim da Cunha, L., Cox, P. M., Eliseev, A. V., Henson, S.,
531 Ishii, M., Jaccard, S., Koven, C., Lohila, A., Patra, P. K., Piao, S., Rogelj, J., Syampungani, S., Zaehle, S., and
532 Zickfeld, K.: Global Carbon and other Biogeochemical Cycles and Feedbacks. In Climate Change 2021: The
533 Physical Science Basis. Contribution of Working Group I to the Sixth Assessment Report of the
534 Intergovernmental Panel on Climate Change [Masson-Delmotte, V., P. Zhai, A. Pirani, S.L. Connors, C. Péan, S.
535 Berger, N. Caud, Y. Chen, L. Goldfarb, M.I. Gomis, M. Huang, K. Leitzell, E. Lonnoy, J.B.R. Matthews, T.K.
536 Maycock, T. Waterfield, O. Yelekçi, R. Yu, and B. Zhou (eds.)], Cambridge University Press, pp. 673–816,
537 doi:10.1017/9781009157896.007, 2021.
- 538 Crespo-Medina, M., Meile, C. D., Hunter, K. S., Diercks, A. R., Asper, V. L., Orphan, V. J., Tavormina, P. L.,
539 Nigro, L. M., Battles, J. J., Chanton, J. P., Shiller, A. M., Joung, D. J., Amon, R. M. W., Bracco, A., Montoya, J.
540 P., Villareal, T. A., Wood, A. M., and Joye, S. B.: The rise and fall of methanotrophy following a deepwater oil-
541 well blowout, *Nature Geoscience*, 7, 423–427, 10.1038/ngeo2156, 2014.
- 542 Duran-Matute, M., Gerkema, T., de Boer, G. J., Nauw, J. J., and Gräwe, U.: Residual circulation and freshwater
543 transport in the Dutch Wadden Sea: a numerical modelling study, *Ocean Sci.*, 10, 611–632, 10.5194/os-10-611-
544 2014, 2014.
- 545 Etmann, M., Myhre, G., Highwood, E. J., and Shine, K. P.: Radiative forcing of carbon dioxide, methane, and
546 nitrous oxide: A significant revision of the methane radiative forcing, *Geophysical Research Letters*, 43, 12,614–
547 612,623, 10.1002/2016gl071930, 2016.
- 548 Gräwe, U., Flöser, G., Gerkema, T., Duran-Matute, M., Badewien, T. H., Schulz, E., and Burchard, H.: A
549 numerical model for the entire Wadden Sea: Skill assessment and analysis of hydrodynamics, *Journal of*
550 *Geophysical Research: Oceans*, 121, 5231–5251, 10.1002/2016jc011655, 2016.
- 551 Green, J. D.: Headspace analysis | Static, in: *Encyclopedia of Analytical Science (Second Edition)*, edited by:
552 Worsfold, P., Townshend, A., and Poole, C., Elsevier, Oxford, 229–236, <https://doi.org/10.1016/B0-12-369397-7/00254-5>, 2005.
- 554 Gründger, F., Probandt, D., Knittel, K., Carrier, V., Kalenitchenko, D., Silyakova, A., Serov, P., Ferré, B.,
555 Svenning, M. M., and Niemann, H.: Seasonal shifts of microbial methane oxidation in Arctic shelf waters above
556 gas seeps, *Limnology and Oceanography*, 66, 1896–1914, <https://doi.org/10.1002/lno.11731>, 2021.
- 557 Grunwald, M., Dellwig, O., Liebezeit, G., Schnetger, B., Reuter, R., and Brumsack, H.-J.: A novel time-series
558 station in the Wadden Sea (NW Germany): First results on continuous nutrient and methane measurements,
559 *Marine Chemistry*, 107, 411–421, 10.1016/j.marchem.2007.04.003, 2007.
- 560 Grunwald, M., Dellwig, O., Beck, M., Dippner, J. W., Freund, J. A., Kohlmeier, C., Schnetger, B., and Brumsack,
561 H.-J.: Methane in the southern North Sea: Sources, spatial distribution and budgets, *Estuarine, Coastal and Shelf*
562 *Science*, 81, 445–456, 10.1016/j.ecss.2008.11.021, 2009.
- 563 Hanson, R. S. and Hanson, T. E.: Methanotrophic Bacteria, *Microbiological reviews*, 60, 439–471, 1996.
- 564 He, R., Wooller, M. J., Pohlman, J. W., Quensen, J., Tiedje, J. M., and Leigh, M. B.: Shifts in Identity and Activity
565 of Methanotrophs in Arctic Lake Sediments in Response to Temperature Changes, *Applied and Environmental*
566 *Microbiology*, 78, 4715–4723, doi:10.1128/AEM.00853-12, 2012.
- 567 Hirayama, H., Fuse, H., Abe, M., Miyazaki, M., Nakamura, T., Nunoura, T., Furushima, Y., Yamamoto, H., and
568 Takai, K.: *Methylomarinum vadi* gen. nov., sp. nov., a methanotroph isolated from two distinct marine
569 environments, *International Journal of Systematic and Evolutionary Microbiology*, 63, 1073–1082,
570 <https://doi.org/10.1099/ijs.0.040568-0>, 2013.
- 571 Ho, A., Mo, Y., Lee, H. J., Sauheitl, L., Jia, Z., and Horn, M. A.: Effect of salt stress on aerobic methane oxidation
572 and associated methanotrophs; a microcosm study of a natural community from a non-saline environment, *Soil*
573 *Biology and Biochemistry*, 125, 210–214, <https://doi.org/10.1016/j.soilbio.2018.07.013>, 2018.
- 574 Jacques, C., Gkritzalis, T., Tison, J.-L., Hartley, T., van der Veen, C., Röckmann, T., Middelburg, J. J., Catruijsse,
575 A., Egger, M., Dehairs, F., and Sapart, C. J.: Carbon and Hydrogen Isotope Signatures of Dissolved Methane in
576 the Scheldt Estuary, *Estuaries and Coasts*, 44, 137–146, 10.1007/s12237-020-00768-3, 2021.
- 577 Jähne, B., Münnich, K. O., Bössinger, R., Dutzi, A., Huber, W., and Libner, P.: On the parameters influencing air-
578 water gas exchange, *Journal of Geophysical Research: Oceans*, 92, 1937–1949,
579 <https://doi.org/10.1029/JC092iC02p01937>, 1987.
- 580 James, R. H., Bousquet, P., Bussmann, I., Haeckel, M., Kipfer, R., Leifer, I., Niemann, H., Ostrovsky, I., Piskozub,
581 J., Rehder, G., Treude, T., Vielstädte, L., and Greinert, J.: Effects of climate change on methane emissions from
582 seafloor sediments in the Arctic Ocean: A review, *Limnology and Oceanography*, 61, S283–S299,
583 10.1002/lno.10307, 2016.
- 584 Jordan, S. F. A., Gräwe, U., Treude, T., van der Lee, E. M., Schneider von Deimling, J., Rehder, G., and Schmale,
585 O.: Pelagic Methane Sink Enhanced by Benthic Methanotrophs Ejected From a Gas Seep, *Geophysical Research*
586 *Letters*, 48, e2021GL094819, <https://doi.org/10.1029/2021GL094819>, 2021.
- 587 Jordan, S. F. A., Treude, T., Leifer, I., Janssen, R., Werner, J., Schulz-Vogt, H., and Schmale, O.: Bubble-mediated
588 transport of benthic microorganisms into the water column: Identification of methanotrophs and implication of
589 seepage intensity on transport efficiency, *Scientific Reports*, 10, 4682, 10.1038/s41598-020-61446-9, 2020.



- 590 Knief, C.: Diversity and Habitat Preferences of Cultivated and Uncultivated Aerobic Methanotrophic Bacteria
591 Evaluated Based on pmoA as Molecular Marker, *Frontier Microbiology*, 6, 1346, 10.3389/fmicb.2015.01346,
592 2015.
- 593 Lan, X., Thoning, K. W., and Dlugokencky, E. J.: Trends in globally-averaged CH₄, N₂O, and SF₆ determined
594 from NOAA Global Monitoring Laboratory measurements, Version 2023-05, [https://doi.org/10.15138/P8XG-](https://doi.org/10.15138/P8XG-AA10)
595 [AA10](https://doi.org/10.15138/P8XG-AA10), 2022.
- 596 Lê, S., Josse, J., and Husson, F.: FactoMineR: An R Package for Multivariate Analysis, *Journal of Statistical*
597 *Software*, 25, 1 - 18, 10.18637/jss.v025.i01, 2008.
- 598 Mariotti, A., Germon, J. C., Hubert, P., Kaiser, P., Letolle, R., Tardieux, A., and Tardieux, P.: Experimental
599 determination of nitrogen kinetic isotope fractionation: Some principles; illustration for the denitrification and
600 nitrification processes, *Plant and Soil*, 62, 413-430, 10.1007/BF02374138, 1981.
- 601 Materić, D., Holzinger, R., and Niemann, H.: Nanoplastics and ultrafine microplastic in the Dutch Wadden Sea –
602 The hidden plastics debris?, *Science of The Total Environment*, 846, 157371,
603 <https://doi.org/10.1016/j.scitotenv.2022.157371>, 2022.
- 604 Mau, S., Blees, J., Helmke, E., Niemann, H., and Damm, E.: Vertical distribution of methane oxidation and
605 methanotrophic response to elevated methane concentrations in stratified waters of the Arctic fjord Storfjorden
606 (Svalbard, Norway), *Biogeosciences*, 10, 6267-6278, 10.5194/bg-10-6267-2013, 2013.
- 607 Middelburg, J. J., Nieuwenhuize, J., Iversen, N., Høgh, N., de Wilde, H., Helder, W., Seifert, R., and Christof, O.:
608 Methane distribution in European tidal estuaries, *Biogeochemistry*, 59, 95-119, 10.1023/A:1015515130419,
609 2002.
- 610 Niemann, H., Steinle, L., Blees, J., Bussmann, I., Treude, T., Krause, S., Elvert, M., and Lehmann, M. F.: Toxic
611 effects of lab-grade butyl rubber stoppers on aerobic methane oxidation, *Limnology and Oceanography*:
612 *Methods*, 13, 40-52, 10.1002/lom3.10005, 2015.
- 613 Osudar, R., Klings, K. W., Wagner, D., and Bussmann, I.: Effect of salinity on microbial methane oxidation in
614 freshwater and marine environments, *Aquatic Microbial Ecology*, 80, 181-192, 2017.
- 615 Osudar, R., Matoušů, A., Alawi, M., Wagner, D., and Bussmann, I.: Environmental factors affecting methane
616 distribution and bacterial methane oxidation in the German Bight (North Sea), *Estuarine, Coastal and Shelf*
617 *Science*, 160, 10-21, <https://doi.org/10.1016/j.ecss.2015.03.028>, 2015.
- 618 Philippart, C. J. M., van Iperen, J. M., Cadée, G. C., and Zuur, A. F.: Long-term Field Observations on Seasonality
619 in Chlorophyll-a Concentrations in a Shallow Coastal Marine Ecosystem, the Wadden Sea, *Estuaries and Coasts*,
620 33, 286-294, 10.1007/s12237-009-9236-y, 2009.
- 621 Reeburgh, W. S.: Oceanic Methane Biogeochemistry, *Chemical Reviews*, 107, 486-513, 10.1021/cr050362v, 2007.
- 622 Röckmann, T., Eyer, S., van der Veen, C., Popa, M. E., Tuzson, B., Monteil, G., Houweling, S., Harris, E.,
623 Brunner, D., Fischer, H., Zazzeri, G., Lowry, D., Nisbet, E. G., Brand, W. A., Necki, J. M., Emmenegger, L.,
624 and Mohn, J.: In situ observations of the isotopic composition of methane at the Cabauw tall tower site,
625 *Atmospheric Chemistry Physics*, 16, 10469-10487, 10.5194/acp-16-10469-2016, 2016.
- 626 Rosentreter, J. A., Borges, A. V., Deemer, B. R., Holgerson, M. A., Liu, S., Song, C., Melack, J., Raymond, P. A.,
627 Duarte, C. M., Allen, G. H., Olefeldt, D., Poulter, B., Battin, T. I., and Eyre, B. D.: Half of global methane
628 emissions come from highly variable aquatic ecosystem sources, *Nature Geoscience*, 14, 225-230,
629 10.1038/s41561-021-00715-2, 2021.
- 630 Røy, H., Lee, J. S., Jansen, S., and de Beer, D.: Tide-driven deep pore-water flow in intertidal sand flats,
631 *Limnology and Oceanography*, 53, 1521-1530, <https://doi.org/10.4319/lo.2008.53.4.1521>, 2008.
- 632 Saunois, M., Stavert, A. R., Poulter, B., Bousquet, P., Canadell, J. G., Jackson, R. B., Raymond, P. A.,
633 Dlugokencky, E. J., Houweling, S., Patra, P. K., Ciais, P., Arora, V. K., Bastviken, D., Bergamaschi, P., Blake,
634 D. R., Brailsford, G., Bruhwiler, L., Carlson, K. M., Carrol, M., Castaldi, S., Chandra, N., Crevoisier, C., Crill,
635 P. M., Covey, K., Curry, C. L., Etiope, G., Frankenberg, C., Gedney, N., Hegglin, M. I., Höglund-Isaksson, L.,
636 Hugelius, G., Ishizawa, M., Ito, A., Janssens-Maenhout, G., Jensen, K. M., Joos, F., Kleinen, T., Krummel, P. B.,
637 Langenfelds, R. L., Laruelle, G. G., Liu, L., Machida, T., Maksyutov, S., McDonald, K. C., McNorton, J.,
638 Miller, P. A., Melton, J. R., Morino, I., Müller, J., Murguía-Flores, F., Naik, V., Niwa, Y., Noce, S., O'Doherty,
639 S., Parker, R. J., Peng, C., Peng, S., Peters, G. P., Prigent, C., Prinn, R., Ramonet, M., Regnier, P., Riley, W. J.,
640 Rosentreter, J. A., Segers, A., Simpson, I. J., Shi, H., Smith, S. J., Steele, L. P., Thornton, B. F., Tian, H.,
641 Tohjima, Y., Tubiello, F. N., Tsuruta, A., Viovy, N., Voulgarakis, A., Weber, T. S., van Wee, M., van der
642 Werf, G. R., Weiss, R. F., Worthy, D., Wunch, D., Yin, Y., Yoshida, Y., Zhang, W., Zhang, Z., Zhao, Y., Zheng,
643 B., Zhu, Q., Zhu, Q., and Zhuang, Q.: The Global Methane Budget 2000–2017, *Earth System Science Data*, 12,
644 1561-1623, 10.5194/essd-12-1561-2020, 2020.
- 645 Schmale, O., Leifer, I., Deimling, J. S. v., Stolle, C., Krause, S., Kießlich, K., Frahm, A., and Treude, T.: Bubble
646 Transport Mechanism: Indications for a gas bubble-mediated inoculation of benthic methanotrophs into the
647 water column, *Continental Shelf Research*, 103, 70-78, 10.1016/j.csr.2015.04.022, 2015.



- 648 Steinle, L., Maltby, J., Treude, T., Kock, A., Bange, H. W., Engbersen, N., Zopfi, J., Lehmann, M. F., and
649 Niemann, H.: Effects of low oxygen concentrations on aerobic methane oxidation in seasonally hypoxic coastal
650 waters, *Biogeosciences*, 14, 1631-1645, 10.5194/bg-14-1631-2017, 2017.
- 651 Steinle, L., Schmidt, M., Bryant, L., Haeckel, M., Linke, P., Sommer, S., Zopfi, J., Lehmann, M. F., Treude, T.,
652 and Niemann, H.: Linked sediment and water-column methanotrophy at a man-made gas blowout in the North
653 Sea: Implications for methane budgeting in seasonally stratified shallow seas, *Limnology and Oceanography*, 61,
654 S367-S386, 10.1002/lno.10388, 2016.
- 655 Steinle, L., Graves, A. C., Treude, T., Ferré, B., Biastoch, A., Bussmann, I., Berndt, C., Krastel, S., James, R. H.,
656 Behrens, E., Böning, C. W., Greinert, J., Sapart, C., Scheinert, M., Sommer, S., Lehmann, M. F., and Niemann,
657 H.: Water column methanotrophy controlled by a rapid oceanographic switch, *Nature Geoscience*, 8, 378-382,
658 10.1038/ngeo2420, 2015.
- 659 Tavormina, P. L., Hatzepichler, R., McGlynn, S., Chadwick, G., Dawson, K. S., Connon, S. A., and Orphan, V.
660 J.: *Methyloprofundus sedimenti* gen. nov., sp. nov., an obligate methanotroph from ocean sediment belonging to
661 the 'deep sea-1' clade of marine methanotrophs, *International Journal of Systematic and Evolutionary*
662 *Microbiology*, 65, 251-259, <https://doi.org/10.1099/ijs.0.062927-0>, 2015.
- 663 Thornton, B. F., Geibel, M. C., Crill, P. M., Humborg, C., and Mörth, C.-M.: Methane fluxes from the sea to the
664 atmosphere across the Siberian shelf seas, *Geophysical Research Letters*, 43, 5869-5877,
665 <https://doi.org/10.1002/2016GL068977>, 2016.
- 666 van Aken, H. M.: Variability of the salinity in the western Wadden Sea on tidal to centennial time scales, *Journal*
667 *of Sea Research*, 59, 121-132, <https://doi.org/10.1016/j.seares.2007.11.001>, 2008.
- 668 Wanninkhof, R.: Relationship between wind speed and gas exchange over the ocean revisited, *Limnology and*
669 *Oceanography: Methods*, 12, 351-362, <https://doi.org/10.4319/lom.2014.12.351>, 2014.
- 670 Weber, T., Wiseman, N. A., and Kock, A.: Global ocean methane emissions dominated by shallow coastal waters,
671 *Nature communications*, 10, 1-10, 2019.
- 672 Whiticar, M. J.: Carbon and hydrogen isotope systematics of bacterial formation and oxidation of methane,
673 *Chemical Geology*, 161, 291-314, [https://doi.org/10.1016/S0009-2541\(99\)00092-3](https://doi.org/10.1016/S0009-2541(99)00092-3), 1999.
- 674 Wiesenberg, D. A. and Guinasso, N. L.: Equilibrium Solubilities of Methane, Carbon Monoxide, and Hydrogen in
675 Water and Sea Water, *Journal of Chemical & Engineering Data*, 24, 356-360, 1979.
- 676 Wu, C. S., Røy, H., and de Beer, D.: Methanogenesis in sediments of an intertidal sand flat in the Wadden Sea,
677 *Estuarine, Coastal and Shelf Science*, 164, 39-45, 10.1016/j.ecss.2015.06.031, 2015.
- 678 Yvon-Durocher, G., Allen, A. P., Bastviken, D., Conrad, R., Gudas, C., St-Pierre, A., Thanh-Duc, N., and del
679 Giorgio, P. A.: Methane fluxes show consistent temperature dependence across microbial to ecosystem scales,
680 *Nature*, 507, 488-491, 10.1038/nature13164, 2014.
- 681 Zhang, S., Yan, L., Cao, J., Wang, K., Luo, Y., Hu, H., Wang, L., Yu, R., Pan, B., Yu, K., Zhao, J., and Bao, Z.:
682 Salinity significantly affects methane oxidation and methanotrophic community in Inner Mongolia lake
683 sediments, *Frontiers in Microbiology*, 13, 10.3389/fmicb.2022.1067017, 2023.

684